Optical properties of Eu^{3+}-doped antimony-oxide-based low phonon disordered matrices

2010 J. Phys.: Condens. Matter 22 035603

(http://iopscience.iop.org/0953-8984/22/3/035603)

J. Phys.: Condens. Matter **22** (2010) 035603 (11pp) doi:10.1088/0953-8984/22/3/035603

Optical properties of Eu^{3+}-doped antimony-oxide-based low phonon disordered matrices

Tirtha Som and Basudeb Karmakar

Glass Technology Laboratory, Glass Division, Central Glass and Ceramic Research Institute (Council of Scientific and Industrial Research), 196 Raja S C Mullick Road, Kolkata 700032, India

E-mail: basudebk@cgcri.res.in

Received 8 September 2009, in final form 17 November 2009
Published 24 December 2009
Online at stacks.iop.org/JPhysCM/22/035603

Abstract

A new series of monolithic Eu_2O_3-doped high antimony oxide (40–80 mol%) content disordered matrices (glasses) of low phonon energy (about 600 cm^{-1}) in the K_2O–B_2O_3–Sb_2O_3 (KBS) system was prepared by the melt–quench technique. Infrared reflection spectroscopy was used to establish the low phonon energy of the glasses. Amorphicity and devitrification of the glasses were confirmed by x-ray diffraction analysis. UV–vis absorption spectra of Eu^{3+} have been measured and the band positions have been justified with quantitative calculation of the nephelauxetic parameter and covalent bonding characteristics of the host. These Eu_2O_3-doped glasses upon excitation at 393 nm radiation exhibit six emission bands in the range 500–750 nm due to their low phonon energy. Of these, the magnetic dipole $^5D_0 \rightarrow {}^7F_1$ transition shows small Stark splitting while the electric dipole $^5D_0 \rightarrow {}^7F_2$ transition undergoes remarkable Stark splitting into two components. They have been explained by the crystal field effect. The Judd–Ofelt parameters, $\Omega_{t=2,4,6}$, were also evaluated and the change of Ω_t with the glass composition was correlated with the asymmetric effect at Eu^{3+} ion sites and the fundamental properties like covalent character and optical basicity. We are the first to report the spectroscopic properties of the Eu^{3+} ion in KBS low phonon antimony glasses.

1. Introduction

Glasses doped with rare earth (RE) ions have emerged as a significant category of solid state luminescent material and are finding ever-increasing applications as compact visible and NIR lasers, broad band amplifiers, light-emitting devices, color display panels, optical data storage, sensors, optical communications, etc [1–3]. In particular, the rising demand in visible laser sources has provoked significant exploitation of RE ions like Eu^{3+}, Sm^{3+}, Dy^{3+}, Tm^{3+} and Pr^{3+} within various disordered matrices [1, 2, 4–6]. Within the rare earth family, trivalent europium (Eu^{3+}) is an important activator for inorganic lattices and is well recognized as a powerful pure red-light-emitting center for display devices due to its dominant $^5D_0 \rightarrow {}^7F_2$ electronic transition [2, 5–15]. The role of the disordered glass environment on the optical properties of rare earth ions is significantly important because it influences the intra-configurational optical transitions. The non-degenerate nature of the (excited) $^5D_0$ and the $^7F_0$ (ground) state and relatively simple energy level system makes Eu^{3+} ions a highly convenient spectroscopic probe for studying the symmetry and inhomogeneity (crystal field effect) present in the host matrices and consequently present valuable information regarding structure and bonding properties of various hosts [16, 17]. In a free Eu^{3+} ion the transitions between the different levels of the $4f^n$ configuration are prohibited by the Laporte selection rule [18]. However, when the Eu^{3+} ions are embedded within a matrix (glass), the ligand field due to the surrounding ions constituting the host perturbs the free ion levels, causing admixing of energy states of different configurations (e.g. $4f^n$ and $4f^{n-1}5d^1$, etc) resulting in non-degeneracy so that the intra-configurational ($4f^n$) transitions become allowed [19]. Slight disparity in the bonding parameters (e.g. ligand distance, ligand angle, coordination number and covalency) causes variation in the strength of the ligand field and consequently in the energy levels of the free ion. Thus, the rare earth absorption

and fluorescence spectra are governed by the local environment around the RE ion.

High transparencies, mechanical strength, ease of fabrication and strong resistance towards atmospheric moisture have helped oxide glasses to emerge as potential hosts for RE ions. As well, heavy metal oxide (HMO) glasses possess some additional advantages like high refractive index, large transmission window, large nonlinear optical properties and, most importantly, low phonon energy. Phonon energy is the lattice vibration in a material that can provide nonradiative decay pathways to suppress luminescence. Thus, low phonon HMO glasses are critical for the reduction of nonradiative losses through multiphonon relaxations, thereby encouraging radiative emissions [7–12]. For the Eu^{3+} ion, since the red fluorescence is due to the transitions from the $^5D_0$ level, which has much higher energy than the next lower level ($^7F_6$), so the phonon energies of the hosts are not a very essential criterion to obtain the red emission [4, 13–17]. However glasses with low phonon energy are advantageous to decrease the multiphonon relaxation rate and obtain efficient radiative emissions from the $^5D_0$ level [7–12]. Besides, the low phonon glasses also provide an opportunity to investigate the unusual emission transitions from the $^5D_1$, $^5D_2$ and $^5D_3$ levels of Eu^{3+} which are rarely observed in hosts of high phonon energy [7, 8].

Although detailed structural and optical investigations have been performed on low phonon HMO glasses like tellurite, lead and bismuth glasses [7–12], to the best of our knowledge there is no report dealing with the fluorescence properties of Eu^{3+}-ion-doped high antimony-oxide-containing glasses along with their infrared reflection spectral study. This is because the Sb^{3+} cation is not a good glass former due to its weak field strength (0.73) [20]. Further, the intense volatilization, crystallization of the melts and, above all, the difficulty in obtaining a monolithic glass have hindered the exploitation of antimony oxide systems particularly in the area of photonics [20]. It is only in recent times that we first reported the systematic analysis of the emission (upconversion) spectra of three different rare earth ions Sm^{3+}, Er^{3+} and Nd^{3+} ions doped separately into antimony oxide (70 mol% Sb_2O_3)-based monolithic glass and they proved to be a very good quality of solid state laser material [21–23]. Sb_2O_3-containing glasses deserve special attention because they are expected to possess a combination of attractive properties like high density, large transmission window (about 0.35–6.5 μm), low phonon energy (600 cm^{-1}), low melting and glass transition temperature, and high linear thermal expansion, even to match those of certain metals and alloys [20]. The development of new glass-based optical devices requires a better perception of the interionic interactions which are deeply associated with the fundamental physics of rare earth ions. The optical properties of RE ions in glasses depend on the chemical composition of the glass matrix which determines the structure and nature of the bonds [24].

Pondering over these issues, in this paper we report a study on the IRRS, UV–vis absorption and photoluminescence downshifting properties of the Eu^{3+} ion in a series of high antimony-oxide-containing glasses having the general composition (mol%) $x K_2O$–$x B_2O_3$–$(100 - 2x)Sb_2O_3$, where $x = 10$–30. Evidence for low phonon energy of the glasses has been provided from the infrared reflection spectra. The emission bands are supported from the evaluation of absorption and excitation spectra, and an energy level diagram. The purpose of this investigation is to obtain a deeper understanding of low phonon antimony glasses and demonstrate the optical properties (luminescence and others) of Eu^{3+} in these glassy hosts, predicting their potential laser properties.

2. Experimental details

The composition (mol%) of the KBS antimony (base) glasses are $x K_2O$–$x B_2O_3$–$(100 - 2x)Sb_2O_3$ glasses, where $x = 10, 15, 20, 25, 30$. The batches were prepared from antimony(III) oxide, Sb_2O_3 (GR, 99%, Loba Chemie), potassium metaborate, KBO_2 (Johnson Matthey) and europium(III) oxide, Eu_2O_3 (99.9%, Alfa Aesar). In order to mix the small quantity of Eu_2O_3 homogeneously to the base glass batch composition, all the raw materials were first mixed carefully in ethanol medium followed by drying. Each batch of 20 g glass doped with 0.7 wt% concentrations of Eu_2O_3 in excess was melted in a high purity silica crucible at 900 °C in air. The molten glass was cast onto a carbon plate and properly annealed. The glasses thus obtained were cut and polished for optical measurement.

The density was measured by the Archimedes method using toluene with an error of ±0.7%. The refractive index and Abbe's number of the base glass were calculated using the Priven-2000 method of SciGlass, 6.7. The x-ray diffraction (XRD) patterns of the bulk samples were recorded in an X'pert Pro MPD diffractometer (PANalytical) operating at 40 kV and 30 mA using Cu kα radiation from 10° to 80°. The infrared reflection spectra (IRRS) in the range 500–1500 cm^{-1} were recorded with a Fourier transform infrared (FTIR) spectrometer at an incident angle of 15° with the help of a specular reflectance measurement accessory attached to the above instrument at the resolution of ±2 cm^{-1} and after 256 scans. The UV–vis absorption spectrum was obtained with a double-beam spectrophotometer (Perkin Elmer, Lambda 20) at an error of ±0.1 nm in band position. Fluorescence spectra were measured, at an error of ±0.2 nm, with a fluorescence spectrophotometer (Spex, Fluorolog 2) in which a xenon lamp is attached as an excitation source and a photomultiplier tube as a detector. All the measurements were carried out at room temperature. The intensity of luminescence was found to be reproducible for all samples.

3. Results and discussion

3.1. Physical properties

Nominal chemical composition and some observed properties of Eu_2O_3-doped KBS antimony glasses are provided in table 1 while some of their calculated properties are provided in table 2. It must be mentioned here that the Eu^{3+}-doped glasses, including the devitrified ones, have been obtained as monoliths and all samples except EU-1 have very good transparencies for

Table 1. Nominal chemical composition and some observed properties of Eu_2O_3-doped KBS antimony glasses.

Sample identity	Composition (mol%) K_2O	B_2O_3	Sb_2O_3	Excess concentration of Eu_2O_3 (wt%)	Density (g cm^{-3})	Color
EU-1	10	10	80	0.7	4.778	Deep yellow
EU-2	15	15	70	0.7	4.576	Yellow
EU-3	20	20	60	0.7	4.361	Yellow
EU-4	25	25	50	0.7	4.115	Pale yellow
EU-5	30	30	40	0.7	3.877	Pale yellow

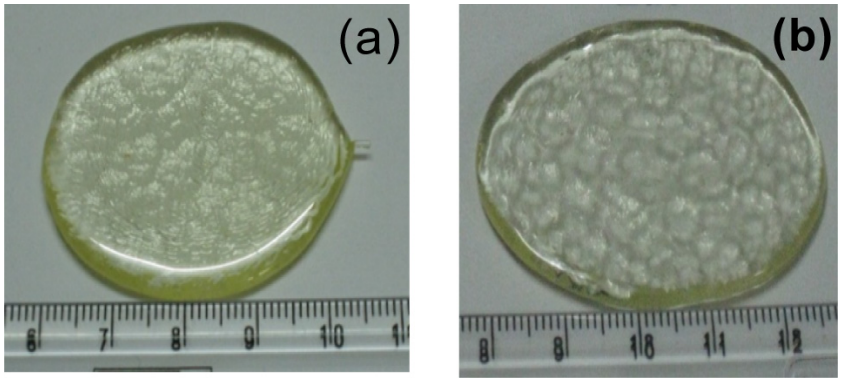

Figure 1. Representative photograph of Eu_2O_3-doped KBS antimony glasses showing their monolithicity: (a) EU-2 and (b) EU-5 (for composition see table 1 and all scales are in cm).

(This figure is in colour only in the electronic version)

optical characterizations. They have a yellow color (figure 1) which decreases with a decrease in Sb_2O_3 content. The yellow color of the glasses is due to the combined effects of host absorption due to transition between HOMO (Sb 5s + O 2pπ) and LUMO (Sb 5p) [20, 21] as well as the extended tails of the charge transfer (CT) band of Eu–O in the range 250–330 nm, i.e. the electron transfer from the valence 2p orbital of O^{2-} to the 4f orbital of the Eu^{3+} ion [11, 13]. Following the procedures reported in our earlier papers [21–23], the Eu^{3+} ion concentration ($N \times 10^{19}$ ions cm^{-3}), interionic distance (r_i, Å) and polaron radii (r_p, Å) were determined and the results are presented in table 2 for easy comparison and better understanding of the effects of the changes in the Eu^{3+} content in the glasses. All the properties listed exhibit the efficiencies of the glasses under investigation as an optical material.

The Eu^{3+} ion concentration per unit volume increases with increasing density of the glasses. Consequently the evaluated data regarding interionic (Eu^{3+}–Eu^{3+}) distance (r_i) and polaron radii (r_p) show a decreasing trend with the change in luminescent ion concentration per unit volume (table 2). Thus, an increase in density of the glasses increases the ionic density and reduces the interionic distance and consequences in narrowing down of the polaron radii [11]. This effect is evidenced as the translucency of sample EU-1 due to lesser solubility of high concentration Eu^{3+} ions in a small volume.

3.2. IRRS spectrum of antimony glasses

The phonon energy ($\hbar\omega$) of glasses is the resonance vibration energy of the lattice and can be estimated by the IRRS. The phonon energy thus corresponds to the highest intensity stretching vibration bond, for example the Si–O–Si bond (1060–1150 cm^{-1}) in silica and silicate glasses, of the network-forming components of the glass [24, 25]. Theoretically, Sb_2O_3-based glasses are expected to have lower phonon energies due to lower stretching vibration of the Sb–O–Sb bond (605 cm^{-1}) [26]. Phonons can provide nonradiative decay pathways to suppress radiative upconversion luminescence of RE ions. Thus, glasses with lower phonon energy are desirable to reduce the multiphonon relaxation and nonradiative loss and to obtain high upconversion efficiency. It is reported that low $\hbar\omega$ of the host can be obtained from the phonon side band (PSB) spectra because the vibration of PSB originates from the local vibration around the RE ions [17, 27]. Although IRRS represents the total vibrations of the whole matrix it provides

Table 2. Some calculated properties of the Eu_2O_3-doped KBS antimony glasses.

Topic	Corresponding values				
Glass no.	EU-1	EU-2	EU-3	EU-4	EU-5
Average molecular weight, M_{av}	250.09	229.20	208.27	187.32	166.36
Eu^{3+} ion concentration, $N \times 10^{19}$ (ions cm^{-3})	11.32	10.84	10.33	9.75	9.18
Interionic distance, r_i (Å)	19.65	20.97	21.31	21.72	22.16
Polaron radius, r_p (Å)	7.92	8.45	8.59	8.76	8.93
Refractive index, n [a]	2.001	1.948	1.892	1.835	1.775
Abbe's number, ν [a]	23.12	23.86	24.80	26.01	27.64

[a] Of KBS base glasses calculated by glass property information system, SciGlass 6.7 (method: Priven-2000).

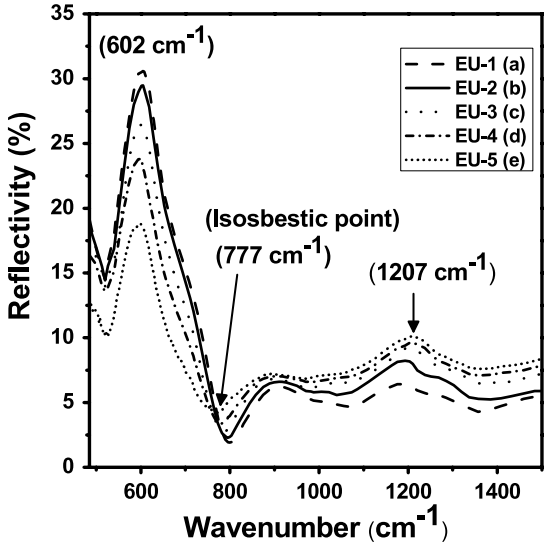

Figure 2. Infrared reflection spectra (FT-IRRS) of base glasses of: (a) EU-1, (b) EU-2, (c) EU-3, (d) EU-4 and (e) EU-5 (for composition see table 1).

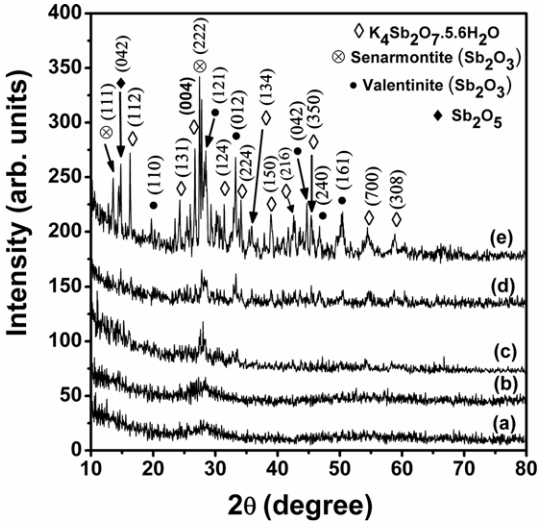

Figure 3. X-ray diffractograms of Eu^{3+}-doped KBS antimony glasses: (a) EU-1, (b) EU-2, (c) EU-3, (d) EU-4 and (e) EU-5 (for composition see table 1).

an alternative way to measure the $\hbar\omega$ of the matrix [25]. The average $\hbar\omega$ values of fluoride glasses obtained by PSB spectra have been found to be very close to those obtained from the low frequency stretching vibrations of IRRS spectra [28]. In addition there are adequate literature reports that document reflection spectra in the infrared (IR) region of 400–1200 cm^{-1} which were measured to establish the phonon energies of the glassy host where the wavenumber at the main peak was cited as the phonon energy of the glass matrix [21–23, 29]. Similarly, we have denoted the main and highest intensity Sb–O–Sb stretching band at 602 cm^{-1} for phonon energy of the KBS antimony glass. It is worth noting that the phonon energy of lead fluoroborate glasses evaluated from Raman spectra corroborates well with those obtained from the main and highest intensity stretching band of infrared spectra as demonstrated by Pisarski *et al* [10]

Figure 2 shows the infrared reflection spectrum (IRRS) of the samples EU1–EU5 in the region 500–1500 cm^{-1}. Two major reflection bands centered at 602 and 1207 cm^{-1} are observed. The highest intensity main reflection band centered at 602 cm^{-1} arises due to Sb–O–Sb stretching vibration [26] while the other one at 1207 cm^{-1} is due to the B–O–B stretching vibration of the $[BO_4]$ unit [30]. The reflection band around 1300 cm^{-1} is due to the B–O–B stretching vibration of the $[BO_3]$ unit [9, 10, 30]. From IRRS spectra $\hbar\omega$ in the high Sb_2O_3 glasses are found to be about 602 cm^{-1}. It is observed that the intensity of the 602 cm^{-1} band decreases with decrease of Sb_2O_3 content and the intensity of the 1207 cm^{-1} band increases indicating an increase in borate content. As a consequence, the IRRS curves show an isosbestic point at 777 cm^{-1} manifesting an existence of equilibrium between the two principal antimony-and boron-containing species.

3.3. X-ray diffraction analysis of the antimony glasses

The x-ray spectrum (figure 3) clearly demarcates the formation of amorphous and devitrified glasses. The hump between $2\theta = 22°$–$35°$ signifies amorphicity. The presence of such a hump and the absence of any peaks in the base glasses EU-1 and EU-2 (curves (a) and (b)) indicates that they have amorphous character and are glasses. It appears that the amount of precipitated Eu_2O_3 in EU-1 is too small to get detected by XRD spectra. The gradual development of sharp peaks in addition to the hump in EU-3, EU-4 and EU-5 (curves (c)–(e)) indicate their devitrified nature. The increasing intensity and decreasing broadness of the peaks as one proceeds from EU-3 to EU-5 indicate intense crystallization with decrease in Sb_2O_3 content. Such intense crystallization is probably due to the large difference in field strengths of Sb^{3+}($F = 0.73$), B^{3+} ($F = 1.34$) and K^+ ($F = 0.13$) ions [20], when the natural and conditional glass former (B_2O_3 and Sb_2O_3, respectively) are present in almost equal amounts.

The XRD spectrum of EU-5 (figure 3, curve (e)) shows prominent peaks due to the development of nanocrystallites of valentinite, senarmontite, Sb_2O_5 and $K_4Sb_2O_7{\cdot}5.65H_2O$ (JCPDS card file nos. 11-689, 43-1071, 34-878 and 35-376, respectively). The corresponding crystallographic planes are assigned in figure 3. The average crystallite diameter (D) is calculated using Scherrer's formula [17]:

$$D = 0.9\lambda/\mathrm{FWHM}\cos 2\theta \ (\mathrm{peak}) \qquad (1)$$

where λ is the wavelength of x-ray radiation (Cu Kα = 1.5406 Å), FWHM is the full width at half-maximum at the angle of diffraction 2θ. The average diameter of the crystallites in EU-3, EU-4 and EU-5 are calculated to be 17, 23 and 33 nm, respectively.

The XRD results clearly support potassium antimony oxide hydrate as the dominant phase with small amounts of crystalline valentinite and senarmontite. The formation of the nanocrystallites introduces a local crystalline environment and perturbs the local site symmetry, resulting in well-resolved Stark splitting in the emission transitions of Eu^{3+} ions when doped in the devitrified glasses, as observed in the emission spectra (see section 3.7).

Table 3. UV–vis absorption band position of Eu^{3+} in KBS antimony glasses and their associated transitions.

	Peak position in						
	Antimony glasses (this study), ±0.1 nm					ZBLANP fluoride glass[a] [32]	Aqueous solution[a] [31]
Transitions	EU-1	EU-2	EU-3	EU-4	EU-5		
$^7F_0 \rightarrow {}^5L_6$	393.9	393.6	393.4	393.1	393.0	393	393.7
$^7F_1 \rightarrow {}^5D_3$		412.0	411.7	411.3	410.9		409.7
$^7F_0 \rightarrow {}^5D_2$		464.5	464.4	464.2	463.6	464	464.7
$^7F_0 \rightarrow {}^5D_1$		525.8	525.7	525.5	525.4	524	525.5
$^7F_1 \rightarrow {}^5D_1$		533.5	533.2	532.7	532.6		535.0

[a] Band positions of Eu^{3+} ion in ZBLANP fluoride glass [$51.5ZrF_4$–$19.5BaF_2$–$5.3LaF_3$–$3.2AlF_3$–$18NaF$–$2.5PbF_2$] and aqueous solution [100 H_2O] are provided for comparison (composition in mol%).

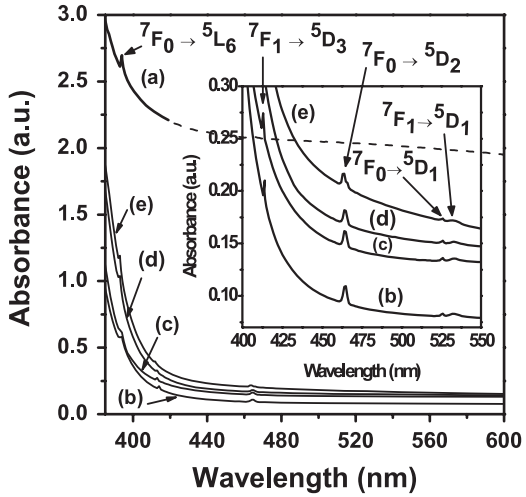

Figure 4. Ultraviolet–visible (UV–vis) absorption spectra of the 0.7 wt% Eu_2O_3-doped KBS antimony glasses: (a) EU-1, (b) EU-2, (c) EU-3, (d) EU-4 and (e) EU-5 (a.u. stands for absorbance unit; for composition, see table 1).

3.4. UV–vis absorption spectra

The ultraviolet–visible (UV–vis) absorption spectrum of each of the 0.7 wt% Eu_2O_3-doped antimony glasses is depicted in figure 4. A total of five absorption bands originating due to $^7F_0 \rightarrow {}^5L_6$, $^7F_1 \rightarrow {}^5D_3$, $^7F_0 \rightarrow {}^5D_2$, $^7F_0 \rightarrow {}^5D_1$ and $^7F_1 \rightarrow {}^5D_1$ are observed. The $^7F_0 \rightarrow {}^5D_2$ absorption band of Eu^{3+} is hypersensitive ($\Delta J = 2$) and its intensity and position are very much susceptible to the local matrix environment. The energy of these absorption bands is assigned on the basis of energy level positions of Eu^{3+} ions in aqueous solution [31] and in other glassy hosts [5–17]. The band positions, λ_{max}, for each Eu^{3+}-doped antimony glass in addition to those obtained in fluoride glass (ZBLANP) [32] and aqueous solution [31] are provided in table 3 to compare and correlate the band position with the covalent bonding characteristics of the hosts.

An interesting aspect of the absorption spectra is that, at low temperatures, only transitions from the ground $^7F_0$ state to the multiplets of ^5D states of the Eu^{3+} ion are observed. But at room temperature transitions from the $^7F_1$ level of the ground state multiplet, which is about 250 cm^{-1} above the $^7F_0$ ground state, are also observed due to thermal population. However, in many glasses the transitions to $^5D_3$ and $^5D_4$ levels are often masked due to strong absorption in the glass [7], although these transitions are reported to be observed in the $LaCl_3$ crystal host [33].

The $^7F_0 \rightarrow {}^5D_1$ transition is also not expected to emerge since an electronic transition from a lower level with $J = 0$ to upper levels with odd J component is forbidden. J-mixing due to the crystal field in the host renders the intra-configurational f–f transition partially allowed. Consequently, in some of our Eu^{3+}-doped antimony glasses this transition is observed but with a very small intensity. Again, since the level $^7F_1$ is close in energy to the $^7F_0$ level, the transitions $^7F_1 \rightarrow {}^5D_1$ appear, however, with a small intensity. Excitingly the $^7F_1 \rightarrow {}^5D_3$ transition appears with a comparatively high intensity.

Since EU-1 contain some precipitated amorphous particles, its absorbance is relatively higher compared to the Eu^{3+}-doped amorphous glass EU-2 due to its turbidity which is the source of scattering (figure 4, curve (a)). The gradual increase in absorbance from EU-2 to EU-5 is due to the development of incipient nanocrystalline phases which act as scattering centers. When the particles are much smaller than the wavelength of visible light ($D \sim \lambda/20$), Rayleigh scattering takes place [34]. The scattering loss or turbidity τ is given by [34]

$$\tau = 32\pi^4 a^3 (n\Delta n)^2 NV/3\lambda^4 \qquad (2)$$

where a is the particle size, λ is the wavelength of light, n is the refractive index, N is the number density of particles and V is the volume of the particles.

3.5. Quantitative justification of UV–vis–NIR absorption band position

Comparison of the absorption band positions of Eu^{3+} ions in antimony hosts with those of fluoride glass and aqueous solution (table 3) shows that the band position shifts towards lower frequency (energy) with the order of host: ZBLANP fluoride glass < KBS antimony glasses < aqueous solution. This shift can be understood in terms of the chemical bonding property of the ligand (here fluorine or oxygen) called the '*nephelauxetic effect*' (literally meaning 'electron cloud expansion') that exerts its influences on the position of the absorption bands. This is a consequence of overlap between the metal and ligand orbitals forming larger molecular orbitals. Ligands with greater ability to delocalize metal electrons shall exhibit higher nephelauxetic effect. Here, it may be noted that

Table 4. Calculated nephelauxetic parameter (B), M–L bonding parameter (δ), electronegativity ($\Delta\chi$), covalent and ionic bonding characteristics and optical basicity (Λ_{th}) of the glasses.

	Corresponding values					
	Antimony glass hosts (this study)				ZBLANP	Aqueous
Topic	EU-2	EU-3	EU-4	EU-5	fluoride glass	solution
Nephelauxetic parameter (B)	0.9999	0.9994	0.9988	0.9983	1.0021	
M–L bonding parameter ($\delta\%$)	0.014	0.057	0.120	0.170	−0.209	
Electronegativity, $\Delta\chi$	1.75	1.80	1.85	1.90	2.8	1.4
Covalent character (%)	46.50	44.49	42.50	40.55	14	61
Ionic character (%)	53.50	55.51	57.50	59.45	86	39
Optical basicity, Λ_{th}	1.035	0.994	0.950	0.901		

the nephelauxetic shift is more largely perceptible for those transitions in which the electric dipole–dipole type interaction dominates.

The electric dipole transitions between the states of the $4f^n$ electron configuration of an isolated Ln^{3+} ion are parity forbidden. However, when such an ion is embedded in a host, it can partially evade this forbiddenness by the noncentrosymmetric interactions with the surroundings (ligands) within the host. Such interactions (chemical bonding) combine states of opposite parity making the transitions feasible. According to Jørgensen [35], owing to '*nephelauxetic effect*', the phenomenological parameters of interelectron repulsion are smaller in a host than in the corresponding free ions. Mathematically, the Hamiltonian operator (H_{fi}) of a free paramagnetic ion can be expressed as

$$H_{fi} = H_{el} + H_{so} + H_{cf}, \tag{3}$$

where H_{el} is the electrostatic interaction of the electron, H_{so} is the spin–orbit interaction and H_{cf} is the interaction of the electrons with the crystal field due to the environment. When an ion is incorporated into a host, due to the nephelauxetic effect, the parameters H_{el}, H_{so} and H_{cf} are reduced from their free-ion values. All these cause a contraction of the energy level structure of the ion in that particular host compared to that of free ion. Consequently, this leads to a shift of the absorption bands towards lower frequency. Quantitatively, this fact can be expressed by the nephelauxetic ratio, β as [23]:

$$\beta = \upsilon_g/\upsilon_a, \tag{4}$$

where υ_g and υ_a are the energy of the corresponding transitions in the glass and aqua ions (or free ion), respectively. The value of the nephelauxetic parameter, B, determining the bonding properties is evaluated from the average values of the (n) observed transitions:

$$B = \left(\sum \upsilon_g/\upsilon_a\right)\Big/ n. \tag{5}$$

The calculated values of B obtained using equation (5) are listed in table 4. The nephelauxetic effect is explained by Jørgensen as an expansion of the partly filled shell ($4f^{n-1}$ of RE ions) due to the transfer of the ligands to the core of the central RE ion. Alternatively it is the measure of the covalency effect. The B value can also be used to determine the metal–ligand (M–L) bonding parameter, δ (in per cent) using the relation [23]

$$\delta\% = [(1 - B)/B] \times 100. \tag{6}$$

The calculated values of $\delta\%$ are also listed in table 4. Depending on the ligand the value of δ may be negative or positive indicating ionic or covalent bonding characteristics respectively. Thus Eu–F bond is predominantly ionic whereas the Eu–O bond has considerable covalent character in addition to ionic character (table 4). A reduced value of B also implies greater covalency in the M–L bond. However, for the same ligand, greater polarizing power of the metal ion implies greater covalency in the M–L bond and hence lower value of B.

The degree of covalent bonding character of a host can be estimated approximately using the formula [20–23]

$$\text{Covalent character (\%)} = \exp[-0.25(\Delta\chi)^2] \times 100, \tag{7}$$

where $\Delta\chi$ is the electronegativity of the glass, that is, the electronegativity difference ($\chi_A - \chi_C$) of the anions and the cations. The average electronegativity of anions (χ_A) or cations (χ_C) can be evaluated by the following simple additive relation [20–23]:

$$\chi_A \text{ or } \chi_C = \Sigma N_i\chi_i/\Sigma N_i, \tag{8}$$

where N_i and χ_i are the number of individual constituent atoms per mole and its electronegativity, respectively. The calculated values of electronegativity, covalent and ionic bonding characteristics of various hosts of the Eu^{3+} ion obtained using equations (7) and (8) are also provided in table 4. In this calculation Pauling's electronegativity values were used.

The Eu^{3+} ion has a smaller ionic radius due to the lanthanide contraction phenomenon and possesses high charge density. It polarizes the comparatively larger O^{2-} more-polarizable anion (electronegativity $\chi_o = 3.5$) to a much greater extent than the smaller F^- less-polarizable anion, obeying Fajan's rules of polarization. This results in a greater extent of molecular orbital overlap between the f orbital of the Eu^{3+} and the p orbital of the O^{2-} ion, resulting in expansion of the electron cloud and the formation of a bond having less ionic and more covalent character (Eu–O has positive $\delta\%$) than that obtained for an M–F bond. Due to the greater

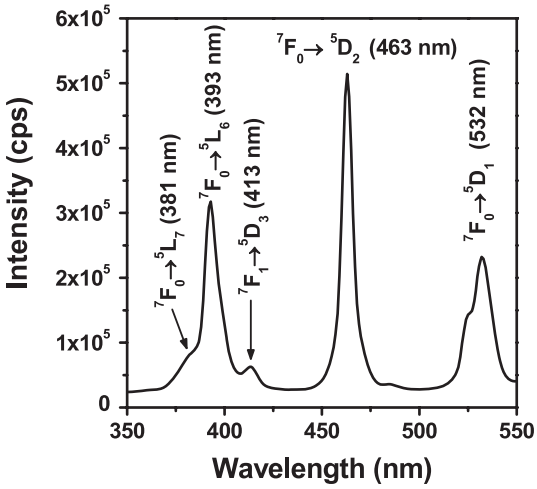

Figure 5. Excitation spectrum with emission at $\lambda_{em} = 617$ nm of the Eu_2O_3-doped KBS antimony glass (EU-2), (cps stands for photon counts per second; for composition see table 1).

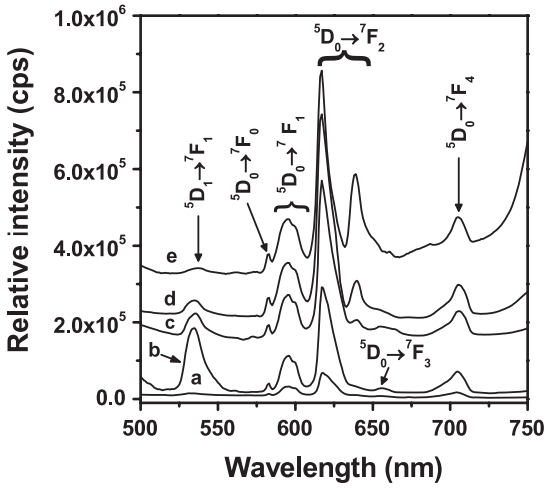

Figure 6. Emission spectra of Eu_2O_3-doped KBS antimony glasses upon excitation at $\lambda_{ex} = 393$ nm radiation: (a) EU-1, (b) EU-2, (c) EU-3, (d) EU-4 and (e) EU-5 (cps stands for photon counts per second; for composition see table 1). The bases of curves b–e have been raised for better visibility.

electronegativity ($\chi_F = 4.0$) and small ionic radius of the F^- ion, the ionic bond results in between Eu^{3+} and F^- ions (Eu–F has negative $\delta\%$). In a similar fashion, the antimony-based glass matrix consisting predominantly of Sb–O and B–O bonds has a greater covalent character. Thus a reliable correlation exists between the nephelauxetic parameter (B) and M–L bonding parameter (δ). This explanation correlated well with those calculated values of electronegativity, covalent and ionic characters of various hosts (see table 4) which bear a significant correlation with the ligand characteristics. Thus, the sequential shifts in positions of the absorption bands are analogous to the shift in covalent character of the host as: ZBLANP fluoride glass < KBS antimony glasses < aqueous solution.

For the same anion (O^{2-}), the variation in covalent character can be interpreted in terms of optical basicity (Λ_{th}). The optical basicity, as proposed by Duffy and Ingram [36], is used as a parameter to determine the acid–base properties of the glass in terms of the electron density carried by oxygen. It represents the average electron donation capacity of the oxide (II) species in the oxide glass after the polarization of their electron charge clouds by constituent cations [11]. The higher the optical basicity, the higher is the covalent character and consequently the greater is the shift of the absorption bands. The theoretical (ideal) optical basicity (Λ_{th}) is calculated according to the expression [36]

$$\Lambda_{th} = X(Sb_2O_3)\Lambda(Sb_2O_3) + X(B_2O_3)\Lambda(B_2O_3) + X(K_2O)\Lambda(K_2O) \quad (9)$$

where $X(Sb_2O_3)$, $X(B_2O_3)$ and $X(K_2O)$ are the equivalent fractions based on the proportion of oxygen, each oxide contributing to the overall glass stoichiometry and $\Lambda(Sb_2O_3) = 1.18$, $\Lambda(B_2O_3) = 0.42$ and $\Lambda(K_2O) = 1.4$ are the basicities assigned to individual oxides [37]. The calculated theoretical optical basicity is shown in table 4. Since Sb_2O_3 has the highest optical basicity or electron donation capacity due to its large size and high polarizability, therefore an increase in equivalent fractions of Sb_2O_3 increases the covalent character.

3.6. Excitation spectra

The excitation spectra (figure 5) reveal five excitation bands at $^7F_0 \rightarrow {}^5D_1$ (532 nm), $^7F_0 \rightarrow {}^5D_2$ (462 nm), $^7F_1 \rightarrow {}^5D_3$ (413 nm), $^7F_0 \rightarrow {}^5L_6$ (393 nm) and $^7F_0 \rightarrow {}^5L_7$ (381 nm) upon excitation at the prominent red emission 617 nm. Among these five excitation wavelengths used in measuring the emission spectra (figure 6), the 393 nm pump wavelength is observed to yield the most intense emission spectral profile. Thus, we consider this to be the best pump wavelength to generate intense red emission from the Eu^{3+}-doped KBS glasses.

3.7. Fluorescence spectra

The fluorescence spectra of Eu^{3+}-doped antimony glasses are shown in figure 6. The emission spectra consist of a series of six emissions bands situated at about 536 (green), 582 (yellow), 595 (orange), 617 (red), 656 (deep-red) and 705 (deep-red) nm. These bands originate due to $^5D_1 \rightarrow {}^7F_1$, $^5D_0 \rightarrow {}^7F_0$, $^5D_0 \rightarrow {}^7F_1$, $^5D_0 \rightarrow {}^7F_2$, $^5D_0 \rightarrow {}^7F_3$ and $^5D_0 \rightarrow {}^7F_4$ electronic transitions, respectively. The $^5D_0 \rightarrow {}^7F_1$ emission transition of Eu^{3+} ions also exhibits small Stark splittings (595 and 600 nm), depending upon the ligand fields being experienced by them. The $^5D_0 \rightarrow {}^7F_2$ transition also shows two distinct main peaks (617 and 639 nm) due to the Stark splitting of the $^7F_2$ state, manifesting that the Eu^{3+} ions are located in drastically disordered lower symmetry sites. The $^5D_0 \rightarrow {}^7F_{2,4}$ emission transitions are identified as electric dipole (ED) which are forced by the crystal field environment in the vicinity of the Eu^{3+} ions [11, 17]. In glassy materials, due to the absence of a center of symmetry and long-range periodic arrangement of atoms, amalgamation of the 4f orbitals with an opposite parity orbital takes place. This gives rise to the ED transitions [11]. Amongst these, the $^5D_0 \rightarrow {}^7F_2$ emission in Eu^{3+} is ED-allowed hypersensitive ($\Delta J = 2$) transition and its intensity is very sensitive to the local environment [11]. For all three samples, the emission spectra are dominated by

Table 5. Relative variation in integrated intensity of downconversion fluorescence bands I_{536}, I_{595} and $I_{617\&639}$ due to $^5D_1 \rightarrow {}^7F_1$ (green), $^5D_0 \rightarrow {}^7F_1$ (orange) and $^5D_0 \rightarrow {}^7F_2$ (red) transitions in Eu_2O_3-doped KBS antimony glasses.

Topic	Corresponding values				
Glass no.	EU-1	EU-2	EU-3	EU-4	EU-5
Downconversion ($\lambda_{ex} = 393$ nm)					
Ratio of I_{536} peak	1	28.7	11.6	7.0	2.1
Ratio of I_{595} peak	1	4.0	4.9	6.0	6.0
Ratio of $I_{617\&639}$ peak	1	4.7	7.9	10.5	13.4
$R = \mathbf{I}(^5D_0 \rightarrow {}^7F_2)/\mathbf{I}(^5D_0 \rightarrow {}^7F_1)$	2.5	2.9	4.0	4.3	5.5

the hypersensitive electric dipole transition $^5D_0 \rightarrow {}^7F_2$ (red emission) over the others. On the other hand, the $^5D_0 \rightarrow {}^7F_1$ transition ($\Delta J = 1$) [11, 17], being a magnetic dipole (MD) allowed, are forbidden under selection rules, has intensity independent of the host environment and thus can be used as a reference. The ratio $R = \mathbf{I}(^5D_0 \rightarrow {}^7F_2)/\mathbf{I}(^5D_0 \rightarrow {}^7F_1)$ of the two integrated fluorescence intensities is commonly used as a measure of the asymmetry around the rare earth sites [9, 10]. The higher the value of R, the greater the deviation from inversion symmetry [10, 38]. Thus, when the Eu^{3+} ions are situated at low symmetry sites, the ED transition has larger probability than the MD transition [39]. Thus, luminescence spectroscopy can be used as a probe to monitor the changes in the Eu^{3+} environment. The larger transition probability of the $^5D_0 \rightarrow {}^7F_2$ hypersensitive transition may correspond to an increase of covalent bonding and bonding strength of the Eu^{3+} with the ligand besides the changes in geometrical arrangement [40]. Despite the increase in covalency and optical basicity, the ratio R is found to be lower for the glasses having a higher proportion of Sb_2O_3, indicating a higher symmetry of sites. Similar behavior has also been demonstrated for CNBZn glasses [40]. Thus, the influence of glass composition on the emission spectra of Eu^{3+} can be expressed by the ratio of the $^5D_0 \rightarrow {}^7F_2$ (red) and $^5D_0 \rightarrow {}^7F_1$ (orange) emission intensities. This ratio is associated with the Judd–Ofelt parameter Ω_2. This parameter is related in turn to the covalency and/or structural changes in the vicinity of Eu^{3+} ions.

The ratio, $R = \mathbf{I}(^5D_0 \rightarrow {}^7F_2)/\mathbf{I}(^5D_0 \rightarrow {}^7F_1)$, varies from 0.90 to 7.04 in different glass compositions [8]. This value in antimony glasses varies in the range 2.5–5.5 (see table 5). The quality of the host material for lasing action is often expressed through the intensity. The ratio provides valuable information about the red color enrichment compared to the orange emission in developing strongly red luminescent optical systems. This indicates the potential of Eu^{3+} doped in antimony glasses as a red laser and phosphor material.

The luminescence spectrum of Eu^{3+} obtained in low phonon glasses is quite dissimilar from those obtained for high phonon hosts [7, 8, 27, 41, 42]. Fluorescence from the higher ^5D levels (e.g. $^5D_1$ and $^5D_2$) of Eu^{3+} are generally obtained in low phonon hosts, have been detected for Eu^{3+} by Weber [40] in LaF_3, by Reisfeld and Lieblich [42] in germanate glasses, and by Todoroki *et al* [27] in fluorophosphate glasses. In our case the fluorescence from the $^5D_1$ level is also observed.

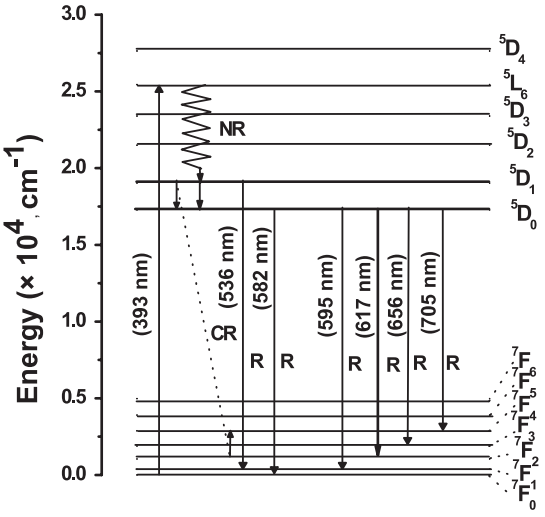

Figure 7. Partial energy level diagram of Eu^{3+}-doped KBS antimony glass (R and NR signify radiative and nonradiative processes, respectively).

The energy level diagram of Eu^{3+} in KBS glass is shown in figure 7. The energy of the $^5L_6$ level of Eu^{3+} is relatively close to the energy for the 393 nm violet radiation and the small mismatch in energy is compensated by the phonon energy of the lattice. Under 393 nm excitation, the Eu^{3+} ions are excited to the $^5L_6$ level by ground state absorption (GSA) from which multiphonon relaxation takes place mainly resulting in the population of the $^5D_0$ and $^5D_1$ levels due to the low phonon energy of the glass. Multiphonon relaxation from the $^5D_0$ level to the next lower level $^7F_6$ does not take place because of the large energy difference ($\sim$12 290 cm^{-1}) between the two levels. According to the Miyakawa–Dexter equation, the rate of multiphonon relaxation processes (W_p) may be expressed as [43]

$$W_p = W_p(0)\exp(-\alpha\Delta E/\hbar\omega) \tag{10}$$

$$\alpha = \ln\{p/g[n(t)+1]\} - 1 \tag{11}$$

$$p \approx \Delta E/\hbar\omega \tag{12}$$

where g is the electron–phonon coupling constant, ΔE is the energy gap between two energy levels ($\sim$12 320 cm^{-1}), $\hbar\omega$ is the phonon energy of the glass host and p is the phonon numbers needed for multiphonon relaxation. From the infrared reflection study we have established that the phonon energy of this KBS glass is about 602 cm^{-1}. This phonon energy is noticeably lower than those of silicate glasses (1060–1150 cm^{-1}), germanate (800–975 cm^{-1}) and tellurite (600–850 cm^{-1}) glasses and is comparable to that of fluoride (500–600 cm^{-1}) glass. Hence a minimum of 20 photons (calculated $p = 20$) are required for bridging the $^5D_0 \rightarrow {}^7F_6$ multiphonon relaxation process. The W_p decreases strongly with increasing p according to equation (10). Thus, the population of the metastable $^5D_1$ and $^5D_0$ levels is greatly increased, leading to high rates of radiative green and red transitions in contrast to those in high phonon energy glasses. Similarly, in this antimony glass host, the population of the metastable $^5D_1$ level is also increased because multiphonon relaxation processes from $^5D_1$ to the next lower $^5D_0$ level require three

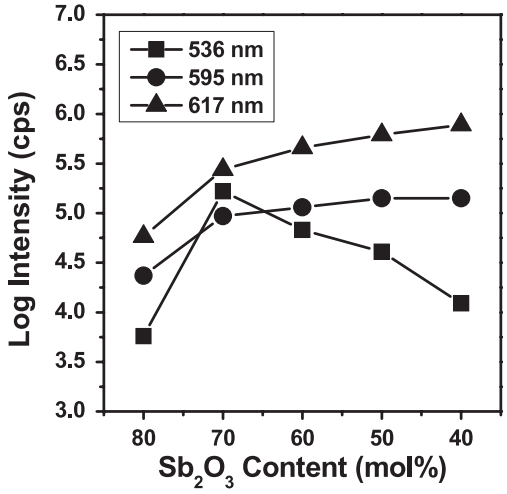

Figure 8. Plot of fluorescence intensity versus concentration of Sb_2O_3 (cps stands for photon counts per second).

bridging phonons. The high phonon orders (phonons $\geqslant 3$) are due to the low phonon energy of the glass host which decreases the possibility of nonradiative multiphonon bridging and consequently manifests the emission $^5D_1 \rightarrow {}^7F_1$ (green) processes (figure 7).

We found that, for the Eu^{3+}-doped glass EU-1, emission performance was drastically reduced. This is attributed to possible cross-relaxation (CR) processes occurring between two neighboring Eu^{3+} ions as $(^5D_1, {}^7F_2) \rightarrow (^7D_0, {}^7F_4)$ due to the smaller interionic distances. This is depicted in figure 7. The intensity variation of the 536 (green), 595 (orange) and 617 (red) nm emission bands with Sb_2O_3 content in the glasses is shown in figure 8.

3.8. Judd–Ofelt theory and calculation of spectroscopic parameters

The Judd–Ofelt (J–O) theory is the most popular method used for spectroscopic investigation of RE ions in various environments [44, 45]. Using the J–O theory, three phenomenological spectroscopic parameters Ω_2, Ω_4 and Ω_6 are experimentally evaluated from the absorption spectra and refractive index of the host material. These parameters can be used to predict the structure around the RE ion sites in a disordered environment and efficiency of the luminescent material. The Eu^{3+} ion faces serious limitations in estimation of the spectroscopic parameters. This is because most transitions are of very weak intensity. Only three well-defined transitions $^7F_0 \rightarrow {}^5D_2$, $^7F_1 \rightarrow {}^5D_3$ and $^7F_0 \rightarrow {}^5L_6$ have been used individually to determine the Judd–Ofelt intensity Ω_2, Ω_4, Ω_6 parameters.

According to the Judd–Ofelt (JO) theory [44, 45] the experimentally measured ED and MD line strength of an electronic transition from an initial $(S, L)J$ state to the final $(S', L')J'$ state is given by

$$S_{\mathrm{ed}}^{\mathrm{med}}(J \rightarrow J') = [9n/(n^2+2)^2] \times \left[\{3ch(2J+1)2.303/8\pi^3 e^2 \rho \lambda_{\max} d\} \times \int_{J\rightarrow J'} OD(\lambda)\,\mathrm{d}\lambda - nS_{\mathrm{med}}\right] \quad (13)$$

where $S_{\mathrm{ed}}^{\mathrm{med}}(J \rightarrow J')$ and S_{med} is the measured ED and MD line strength, $\lambda_{\max}$ is the mean wavelength of the absorption band, n is the refractive index of the host, d is the thickness of the sample under study, ρ is the concentration of Eu^{3+} ions (ions cm^{-3}) in the host and $\int_{J\rightarrow J'} OD(\lambda)\,\mathrm{d}\lambda$ represents the experimental integrated optical density in the wavelength range of the band and can be obtained by calculating the total area under the band. To calculate the integrated absorption of the bands, a base-glass-corrected absorption spectrum was used after necessary correction for the overall rise in the baseline. Since the three transitions $^7F_0 \rightarrow {}^5D_2$, $^7F_1 \rightarrow {}^5D_3$ and $^7F_0 \rightarrow {}^5L_6$ are induced by ED, so the MD term is neglected.

The theoretical electric dipole line strength of an electronic transition from an initial $(S, L)J$ state to the final $(S', L')J'$ state is given by [3]

$$S_{\mathrm{ed}}^{\mathrm{theo}} = \sum \Omega_{t(=2,4,6)} |\langle (S, L)J||U^t||(S', L')J'\rangle|^2 \quad (14)$$

where $\langle (S, L)J||U^t||(S', L')J'\rangle|$ is the reduced matrix element of the irreducible tensor operator of rank t calculated in the intermediate coupling approximation for the transitions, almost invariant with respect to crystal field strength and depends only on the concerned RE^{3+} ion. The values of the square of the reduced matrix elements for various transitions of Eu^{3+} ions are obtained from the literature [31].

Using the above two equations and considering the $^7F_0 \rightarrow {}^5D_2$, $^7F_1 \rightarrow {}^5D_3$ and $^7F_0 \rightarrow {}^5L_6$ transitions, the three Judd–Ofelt parameters Ω_t ($t = 2, 4$ and 6) of the Eu^{3+} ion in the glasses were calculated and presented in table 6 to compare with other glasses. These three intensity parameters originate from a static crystal field and bear a physical significance relevant to the fundamental properties of the host matrix. The parameter Ω_2 implicates the asymmetry around the rare earth ion and is sensitive to the asymmetry of the ligand field. So Ω_2 can be used to draw inferences regarding variation between Eu^{3+} ion sites in various hosts. The parameter Ω_2 is also critically influenced by the covalency between rare earth ions and ligand anions, i.e. Eu–O bond [46]. Generally the parameter Ω_2 increases with the asymmetry of the local structure [1, 17] and with the decrease of covalency of the lanthanide–ligand bonds [17, 46]. However, it is seen that the value of Ω_2 remains almost constant with the change in glass composition. This indicates a delicate balance between the asymmetry effect and covalent character. The covalent character decreases with the decrease in Sb_2O_3 content. However, for the devitrified glasses containing a lower concentration of Sb_2O_3 there is a higher degree of asymmetry around the rare earth ion. This is in agreement with the XRD and luminescence spectra. As the Sb_2O_3 content decreases, devitrification of the glasses occurs. As a result the Eu^{3+} ions find themselves in a high like-crystalline environment. Consequently the luminescence spectra show well-resolved Stark components. High values of Ω_2 ($\Omega_2 > 2$) suggest a highly asymmetric coordination environment [47] and this implies to our case. It has also been documented that Ω_2 is closely connected with the hypersensitive transitions [24]. The greater the hypersensitive transition, the larger is the value of Ω_2. For the Eu^{3+} ion, the transition $^7F_0 \rightarrow {}^5D_2$

Table 6. Comparison of Judd–Ofelt parameters ($\Omega_{t(t=2,4,6)} \times 10^{-20}$ cm^2) of Eu^{3+}-doped KBS antimony oxide glasses with other different glasses.

Host (glass) matrix	Ω_2	Ω_4	Ω_6	Ω_4/Ω_6	Reference
ZBLAN:Eu^{3+}	0.05	1.34	1.61	0.83	[15]
$60NaPO_3$–$15BaF_2$–$10YF_3$–$15EuF_3$	3.24	5.11	2.89	1.77	[16]
$10K_2O$–$30MgO$–$60SiO_2$:Eu^{3+}	9.65	6.68	1.15	5.81	[14]
$79TeO_2$–$20Li_2CO_3$–$1Eu_2O_3$	11.06	4.58	0.96	4.77	[8]
$75NaPO_3$–$24ZnF_2$–$1EuF_3$	6.8	6.2	4.2	1.48	[6]
EU-2	6.9	6.1	9.4	0.65	Present study
EU-3	7.0	4.6	8.6	0.53	Present study
EU-4	7.0	3.1	7.5	0.41	Present study
EU-5	7.1	2.1	7.2	0.29	Present study

is hypersensitive with a relatively higher value of $||U^2||^2 = 0.0008$. Again, since only the $||U^2||^2$ term affects the line strength of the $^5D_0 \rightarrow {}^7F_2$ transition, the intensity ratio $R = \mathbf{I}(^5D_0 \rightarrow {}^7F_2)/\mathbf{I}(^5D_0 \rightarrow {}^7F_1)$ is the measure of Ω_2 [24]. Higher values for Ω_2 and hence high radiative rates are found in highly covalent (highly polarizable) glasses. Potassium boron antimony oxide (KBS) glasses having covalent bonding character therefore show strongly increased intensity of this transition.

The physical implication of Ω_4 and Ω_6 is relatively indistinct. It has been suggested that the magnitudes of Ω_4 and Ω_6 are not only influenced by the rigidity and packing fraction of the glass network surrounding the rare earth ion [48] but also related to the bulk properties of the samples and influenced by the vibronic transitions of the RE ion–ligand bond [48]. In fact, they are also sensitive to the structural changes [24]. It is also suggested that the Ω_6 parameter is inversely proportional to the degree of covalency of the Eu–O bond [1] and/or with the increase of the fraction of nonbridging oxygen ions [3] and should decrease with the electronic density of the O^{2-} ion, that is, optical basicity [24]. In the present case both Ω_4 and Ω_6 are found to increase in glasses having a higher proportion of Sb_2O_3. It can therefore be concluded that the structural changes in the glasses due to devitrification significantly take precedence over the covalency effect.

Table 6 reveals that Ω_6 has a higher value compared to the other two parameters in all the glasses. The ratio (Ω_4/Ω_6) is known as the spectroscopic quality factor to characterize the quality of the luminescent material concerned [1, 49]. Determination of the spectroscopic quality factor in the glasses helps to maximize certain desirable radiative transitions in a laser by changing the branching ratio with variation of the Ω_4/Ω_6 ratio. Based on the magnitudes of the spectroscopic quality factor (Ω_4/Ω_6), it is found that Eu-doped KBS glasses are potentially good quality laser materials. The variation of the Ω_4/Ω_6 ratio on passing from one glass to another indicates the change in the average coordination around the Eu^{3+} ion due to change in the nanocrystalline environment and thereby the average crystal field experienced by the ions.

4. Conclusions

We obtain a deeper understanding of a new low phonon antimony-based oxide glass system K_2O–B_2O_3–Sb_2O_3 (KBS) doped with Eu_2O_3. Infrared reflection spectroscopy has proved that these disordered matrices have a low phonon energy of about 600 cm^{-1}. X-ray diffraction analysis has established the devitrification of some glasses. UV–vis absorption band positions have been measured and justified with quantitative calculation of the nephelauxetic parameter, covalency and optical basicity of the host. Upon excitation at 393 nm radiation, these Eu_2O_3-doped glasses exhibit six emission bands at 536 (green), 582 (yellow), 595 (orange), 617 (red), 656 (deep-red) and 705 (deep-red) nm due to $^5D_1 \rightarrow {}^7F_1$, $^5D_0 \rightarrow {}^7F_0$, $^5D_0 \rightarrow {}^7F_1$, $^5D_0 \rightarrow {}^7F_2$, $^5D_0 \rightarrow {}^7F_3$ and $^5D_0 \rightarrow {}^7F_4$ electronic transitions. The 536 nm band essentially arises due to the low phonon energy of the host. Both the electric ($^5D_0 \rightarrow {}^7F_2$) and magnetic ($^5D_0 \rightarrow {}^7F_1$) dipoles show prominent Stark splitting into two components. These have been explained by the crystal field effect and low phonon energy of the host. The Judd–Ofelt parameters were also evaluated and their variation has been explained by the covalent character, optical basicity and noncentrosymmetry of the Eu^{3+} ion sites. These Eu^{3+}-doped glasses appear to be promising for red laser source application.

Acknowledgments

TS gratefully acknowledges the financial support of the Council of Scientific and Industrial Research (CSIR), New Delhi in the form of NET-SRF under sanction no. 31/015(0060)/2007-EMR-1. The authors gratefully thank Dr H S Maiti, Director of the institute for his kind permission to publish this paper. The technical support (XRD) provided by the infrastructural facility of this institute is also gratefully acknowledged.

References

[1] Qiao X, Fan X, Wang M, Adam J L and Zhang X 2006 *J. Phys.: Condens. Matter* **18** 6937–51
[2] Lin H, Yang D, Liu G, Ma T, Zhai B, An Q, Yu J, Wang X, Liu X and Pun E Y B 2005 *J. Lumin.* **113** 121–8
[3] Feng X, Tanabe S and Hanada T 2001 *J. Am. Ceram. Soc.* **84** 165–71
[4] Pisarski W A, Pisarska J, Dominiak-Dzik G and Ryba-Romanowski W 2004 *J. Phys.: Condens. Matter* **16** 6171–84
[5] Lin H, Pun E Y B, Wang X and Liu X 2005 *J. Alloys Compounds* **390** 197–201
[6] Deun R V, Binnemans K, Görller-Walrand C and Adam J L 1998 *J. Phys.: Condens. Matter* **10** 7231–41
[7] Lin H, Tanabe S, Lin L, Yang D L, Liu K, Wong W H, Yu J Y and Pun E Y B 2006 *Phys. Lett.* A **358** 474–7

[8] Kumar A, Rai D K and Rai S B 2002 *Spectrochim. Acta* A **58** 2115–25
[9] Pisarski W A, Pisarska J, Dominiak-Dzik G, Mączka M and Ryba-Romanowski W 2006 *J. Phys. Chem. Solids* **67** 2452–7
[10] Pisarski W A, Pisarska J, Mączka M and Ryba-Romanowski W 2006 *J. Mol. Struct.* **792/793** 207–11
[11] Kam C H and Buddhudu S 2004 *J. Quantum Spectrosc. Radiat. Trans.* **87** 325–37
[12] Babu S S, Jang K, Cho E J, Lee H and Jayashanksar C K 2007 *J. Phys. D: Appl. Phys.* **40** 5767–74
[13] Chakrabarti R, Das M, Karmakar B, Anapurna K and Buddhudu S 2007 *J. Non-Cryst. Solids* **353** 1422–6
[14] Nageno Y, Takebe H, Morinaga K and Izumitani T 1994 *J. Non-Cryst. Solids* **169** 288–94
[15] McDougall J, Hollis D B and Payne M J P 1994 *Phys. Chem. Glasses* **35** 258–9
[16] Balda R, Fernandez J, Adam J L and Arriandiaga M A 1996 *Phys. Rev.* B **54** 12076–86
[17] Zhao D, Qiao X, Fan X and Wang M 2007 *Physica* B **395** 10–5
[18] Reisfeld R 1975 *Struct. Bonding* **22** 123–75
[19] Layne C B and Weber M J 1977 *Phys. Rev.* B **16** 3259–61
[20] Som T and Karmakar B 2009 *J. Am. Ceram. Soc.* **92** 2230–6
[21] Som T and Karmakar B 2008 *J. Lumin.* **128** 1989–96
[22] Som T and Karmakar B 2009 *Opt. Mater.* **31** 609–18
[23] Som T and Karmakar B 2009 *J. Alloys Compounds* **476** 383–9
[24] Tanabe S, Ohyagi T, Soga N and Hanada T 1992 *Phys. Rev.* B **46** 3305–10
[25] Cases R and Chamarro M A 1991 *J. Solid State Chem.* **90** 313–9
[26] Miller P J and Cody C A 1982 *Spectrochim. Acta* A **38** 555–9
[27] Todoroki S, Tanabe S, Hirao K and Soga N 1991 *J. Non-Cryst. Solids* **136** 213–8
[28] Soga K, Inoue H, Makishima A and Inoue S 1993 *J. Lumin.* **55** 17–24
[29] Murata T, Takebe H and Morinaga K 1998 *J. Am. Ceram. Soc.* **81** 249–51
[30] Kamitsos E I, Patsis A P and Chryssikos G D 1993 *J. Non-Cryst. Solids* **152** 246–57
[31] Carnall W T, Fields P R and Rajnak K 1968 *J. Chem. Phys.* **49** 4450–5
[32] France P W, Drexhage M G, Parker J M, Moore M W, Carter S F and Wright J V 2000 *Fluoride Glass Optical Fibers* (Boca Raton, FL: Blacie, CRC Press)
[33] DeShazer L G and Dieke G H 1963 *J. Chem. Phys.* **38** 2190
[34] Dejneka M J 1998 *J. Non-Cryst. Solids* **239** 149–55
[35] Jørgensen C K 1971 *Modern Aspects of Ligand Field Theory* (Amsterdam: North-Holland)
[36] Duffy J A and Ingram M D 1991 *Optical Properties of Glass* ed D Uhlman and N Kreidl (Westerville, OH: American Ceramic Society) p 159
[37] Dimitrov V and Komatshu T 1999 *J. Ceram. Soc. Japan* **107** 879–86
[38] Brow R K, Tallant D R and Turner G L 1996 *J. Am. Ceram. Soc.* **79** 2410–6
[39] Fan X, Wu X, Wang M, Qiu J and Kawamoto Y 2004 *Mater. Lett.* **58** 2217–21
[40] Weber M J 1967 *Optical Properties of Ions in Crystals* ed H M Crosswhite and H W Moos (New York: Wiley–Interscience) p 467
[41] Balda R, Fernandez A J, Gracia A J and Imbusch G F 1995 *J. Lumin.* **76/77** 551–4
[42] Reisfeld R and Lieblich N 1973 *J. Phys. Chem. Solids* **34** 1467
[43] Miyakawa T and Dexter D L 1970 *Phys. Rev.* B **1** 2961–9
[44] Judd B R 1963 *Phys. Rev.* **127** 750–61
[45] Ofelt G S 1962 *J. Chem. Phys.* **37** 511
[46] Nageno Y, Takebe H and Morinaga K 1993 *J. Am. Ceram. Soc.* **76** 3081–6
[47] Jiang Z, Jianhu Y and Shixun D 2004 *J. Opt. Soc. Am.* B **21** 739–43
[48] Nazabal V, Todoroki S, Nukui A, Matsumoto T and Suehara S 2003 *J. Non-Cryst. Solids* **325** 85–102
[49] Kaminskii A A 1990 *Laser Crystals, Their Physics and Properties* 2nd edn (Berlin: Springer)